Chem Soc Rev

TUTORIAL REVIEW

Engineering plasmonic metal colloids through composition and structural design

Cite this: DOI: 10.1039/c3cs60347d

N. E. Motl,[a] A. F. Smith,[ab] C. J. DeSantis[a] and S. E. Skrabalak*[a]

Received 1st October 2013

DOI: 10.1039/c3cs60347d

www.rsc.org/csr

The optical properties of metal nanomaterials are determined by a set of parameters that include composition, particle size and shape, overall architecture, and local environment. This Tutorial Review examines the influence of each of these factors on the localized surface plasmon resonance of colloidal metal nanoparticles. This examination is paralleled with a discussion of the advances which have enabled the synthesis of structurally defined metal nanomaterials, as these samples serve as the best platforms for elucidating the fundamental properties of plasmonic colloids. Based on the analysis of such samples, five guidelines are presented to aid the rational design and synthesis of new metal nanostructures for advanced applications in nanomedicine, energy, chemical sensing, and colloidal plasmonics in general.

Key learning points

- Plasmonic colloids are metal nanoparticles with sizes close to or less than the wavelength of light; they display localized surface plasmon resonances in which light is scattered and absorbed at specific wavelengths.
- The optical properties displayed by plasmonic colloids are a function of composition, particle size and shape, overall architecture, and surrounding environment.
- The shape and architecture of metal nanocrystals can be controlled through selection of an appropriate seed structure and capping agent as well as manipulation of nanocrystal growth kinetics.
- Although Au and Ag nanostructures are the most widely studied plasmonic colloids, new opportunities and function are emerging from bimetallic nanostructures.
- Plasmonic colloids are finding use in nanomedicine, chemical sensing, energy applications, and more.

Introduction

Humans are visually oriented and thus fascinated by interactions of light with matter. For example, noble metal nanoparticles have long been used by artists to provide coloration for stained glass windows and metallic luster in ceramics. A more recent example of the artistic applications of these materials is shown in Fig. 1, where Ag nanoparticles were deposited on a glass surface to provide a dynamic viewing experience in which the colors observed depend on both the movement of the observer relative to the piece and the light incident.[1] The vibrant colors of metal colloids were first postulated by Michael Faraday to be a consequence of the interaction of light with the nanoscale features of the material and were later described in terms of classical electrodynamics in the seminal work by Gustave Mie.[2]

In recent years, the light–matter interactions of noble metal nanomaterials have garnered interest for use in a variety of applications. Au nanoparticles, for example, are addressing needs in the areas of human health and medicine. The optical properties that result from their nanoscale dimensions, combined with the general biocompatibility of Au, are enabling their use in *in vitro* diagnostics, *in vivo* imaging, photothermal therapy, drug delivery and more, as described by Dreaden *et al.* and the references therein.[3] Additionally, nanoscale optical phenomena are driving the fabrication of waveguides which allow for the manipulation of light at dimensions below the diffraction limit of classical optics.[4] The optical properties of noble metal nanostructures also offer platforms for plasmon-enhanced surface spectroscopies, with the promise of single molecule detection and in various sensing applications.[5]

The diversity of applications possible with metal colloids arises from the small sizes of nanomaterial features relative to the wavelength of incident light. The interaction of light with metal surfaces results in coupling between the free electrons of the metal and the incident light to yield a coherent oscillation

[a] Department of Chemistry, Indiana University, Bloomington, Indiana 47405, USA. E-mail: sskrabal@indiana.edu
[b] NAVSEA Crane, Crane, Indiana 47522, USA

of the free electrons. When the metal is confined to nanoscale dimensions; *i.e.* a metallic nanoparticle, this coherent oscillation of electrons is localized and the frequency of oscillation is referred to as the localized surface plasmon resonance (LSPR).[2] A schematic of this process is shown in Fig. 2A. These oscillations are associated with enhancement of the electromagnetic field locally near the nanoparticle surface,[2,6] and the sustained LSPR of metallic nanoparticles enables a variety of applications. Remarkably, the composition, size, shape, and architecture of these plasmonic nanomaterials can be modified to generate tunable LSPR features. Examples of this capability are shown in Fig. 2B.[3]

As plasmonic nanomaterials see more applications, the ability to selectively tune the LSPR features that result from these materials becomes increasingly important. The exact optical properties of these materials depend on the size, shape, and composition of the nanostructure as well as the environment that it experiences. Understanding how these parameters affect the LSPR has been a topic of interest for many years, with a variety of metal nanoparticles of different morphologies being reported in efforts to understand how the features of the LSPR are affected by changes in nanoparticle structure (Fig. 3).[7] As the behavior of these materials is complex and affected by multiple factors, a more holistic approach to the design of future plasmonic systems has been recommended.[8]

This tutorial will discuss the factors that influence the LSPR of colloidal metal nanoparticles, beginning with an examination

N. E. Motl

Dr Nathan Motl received his BS in chemistry from Southern Illinois University – Edwardsville in 2007 where he was the recipient of a number of awards, including the 2006 and 2007 Thomas D. Bouman Research Awards for his accomplishments with Professor Michael Shaw. He received his PhD in chemistry from the Pennsylvania State University with Professor Raymond Schaak in 2012. He is currently working with Professor Sara Skrabalak as a postdoctoral fellow at Indiana University. His current research interests include shape, composition and architectural control of inorganic nanoparticles, electrochemistry, catalysis, plasmonics and nanotechnology.

A. F. Smith

Alison Smith received her BS in Chemistry and Mathematics at Southeastern Louisiana University, where she performed research on conductive polymers with Professor Brad Wurm; her MEd in Secondary Science Education at Louisiana State University, where she conducted research on stimuli-responsive materials with Robin McCarley; and her MS in Materials Science and Engineering at University of Florida, where she conducted research on cathode materials with Professor Kevin Jones. She is employed by NAVSEA Crane and is working on her PhD at Indiana University with Professor Sara Skrabalak. Her research interests include optical properties of bimetallic nanocrystals and assembly of nanocrystals via template methods.

C. J. DeSantis

Christopher DeSantis received his BS in Chemistry at the Pennsylvania State University where he conducted solid-state research with Professor Raymond Schaak. He is currently a PhD candidate at Indiana University with Professor Sara Skrabalak. He is the recipient of the Chester Davis Fellowship in inorganic chemistry and the Raymond Siedle Fellowship in materials chemistry, both from Indiana University. His research interests include the study of noble metal nanoparticle synthesis, including branched and concave architectures, through seed-mediated co-reduction and their optical and catalytic properties.

S. E. Skrabalak

Dr Sara Skrabalak received her BA in chemistry from Washington University in St. Louis where she conducted research with Professor William Buhro. She completed her PhD in chemistry from the University of Illinois at Urbana-Champaign under the tutelage of Professor Kenneth Suslick. She then conducted post-doctoral research at the University of Washington – Seattle with Professor Younan Xia. She is an Assistant Professor of Chemistry at Indiana University and a recipient of both NSF and DOE CAREER Awards. She is a Research Corporation Cottrell Scholar, a Sloan Research Fellow, and the recipient of the 2014 ACS Award in Pure Chemistry. Her research group focuses on nanomaterial design and synthesis (http://www.indiana.edu/~skrablab/).

Fig. 1 "Through the Looking Glass 1" by Kate Nichols. Nichols created this piece by synthesizing Ag nanoparticles and depositing them on glass. Image used with permission from ref. 1.

of both particle size and composition. On account of the limited ability to manipulate the optical properties of quasi-spherical metal colloids through these two parameters alone, the opportunities enabled with shape-controlled metal nanocrystals will be highlighted next. Finally, the tutorial will conclude with a discussion of platforms in which shape and composition have been brought together into individual nanostructures to achieve new opportunities in colloidal plasmonics. This structure parallels the historical advances in the synthesis of metal colloids, beginning with the size-controlled metal nanoparticles achieved by Faraday in 1857 then shape-controlled metal nanocrystals achieved from the 1990s to the present and finally the architecturally controlled bimetallic nanostructures just now being realized. The common synthetic strategies that enable various high-quality metal colloids to be achieved will be discussed within each section. It is our goal to provide design criteria toward the rational construction of new colloidal plasmonic platforms for the next generation of applications.

Gold, silver, and beyond: the importance of composition and particle size

From the perspective of design, selecting the material that will serve as the plasmonic base is a logical first step. In practice, nanoparticles composed of Ag or Au are the most studied. This focus arises on account of the ease with which high-quality nanoparticle samples composed of these metals can be synthesized. Also, Au and Ag nanoparticles have peak plasmon

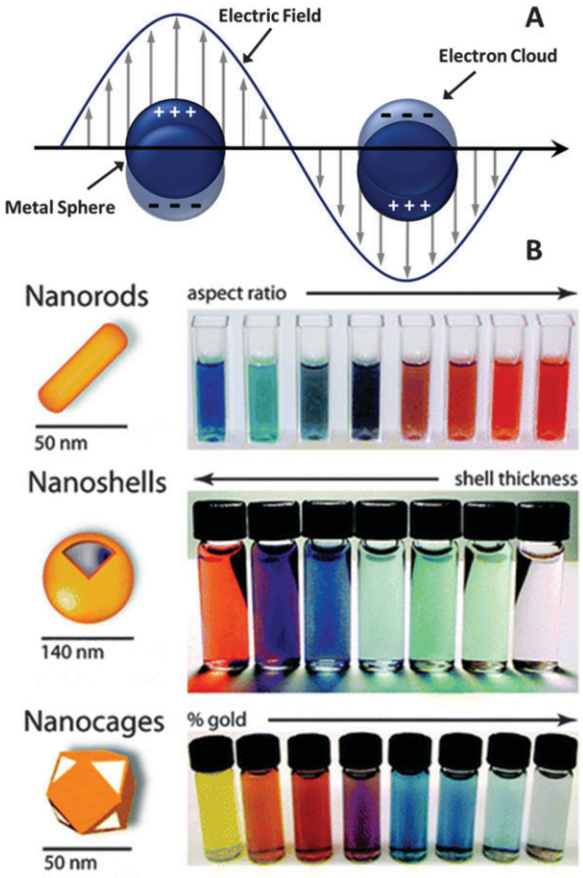

Fig. 2 (A) Schematic illustrating a localized surface plasmon on a metal nanoparticle. (B) Figure that illustrates relationships between shape, architecture, and composition (from top to bottom) on the optical properties of metal nanoparticles (Au nanorods, nanoshells, and nanocages, respectively). Used with permission from ref. 3. Copyright 2007 The Royal Society of Chemistry.

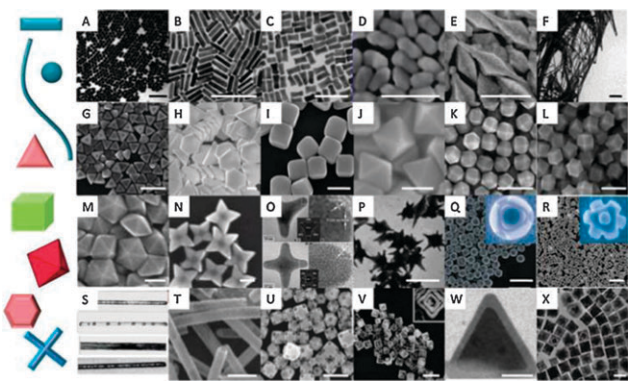

Fig. 3 Collage of scanning and transmission electron microscopy (SEM and TEM) images of noble metal nanocrystal geometries available. Reproduced with permission from ref. 7. Copyright 2012 Elsevier Ltd.

frequencies in the visible region of the spectrum where the resonant condition for polarizability is met and the electromagnetic field is enhanced. Such high-quality samples are achieved by either thermal decomposition or reduction of metal precursors in the presence of capping agents which can

coordinate to their surfaces. The capping agents provide morphological, compositional, and colloidal stability to the generated metal colloids, and size control is achieved *via* reaction conditions such as metal precursor concentration relative to the number of seeds nucleated in the initial stages of a synthesis.[9,10] By manipulating the size of the metal nanoparticles, the position of their LSPR can be tuned over a narrow range within the visible region for these metals, where plasmon excitations can be accomplished using standard optical sources.[2,8] Other metals that exhibit LSPRs in the ultraviolet range – such as Al, Ga, In, Sn, Tl, Pb, and Bi – have also been investigated and will be discussed later in greater detail.[11]

The LSPR frequency associated with metal nanoparticles depends on the complex dielectric function of the material.[2] A localized surface plasmon can exist at any interface in which the real components of the dielectrics of the two materials comprising the interface have opposite signs. This feature is evident from eqn (1) which describes the electromagnetic field outside of a spherical particle, E_{out}, and is obtained by solving Maxwell's equations using a quasi-static approximation.[2] Unit vectors along the Cartesian axes x, y, and z are denoted as $\hat{x}\,\hat{y}$, $\hat{z}$. In eqn (1), E_0 is the incident field polarized in the z-direction, a and r are the radius of the particle, ε_{in} is the dielectric constant of the metal nanoparticle, and ε_{out} is the dielectric constant of the medium. The resonant condition for polarizability is met when the real part of the dielectric is roughly equal to $-2\varepsilon_{out}$,[2,6] and this condition is where the electromagnetic field is maximally enhanced.

The EM field outside the particle.

$$E_{out}(x,y,z) = E_0\hat{z} - \left[\frac{\varepsilon_{in}-\varepsilon_{out}}{\varepsilon_{in}+2\varepsilon_{out}}\right]a^3E_0\left[\frac{\hat{z}}{r^3} - \frac{3z}{r^5}(x\hat{x}+y\hat{y}+z\hat{z})\right] \quad (1)$$

It is worth noting that the dielectric function of a metal is dependent on wavelength (eqn (2)). Maxwell's equations describe light interactions with materials at the material–medium interface, and the Mie solution to Maxwell's equations can describe the scattering of light by metallic nanoparticles with spherical shape. The LSPR of metallic nanoparticles are observed *via* these scattering events. The Mie solution has been successfully applied to describe such scattering events and predict or simulate extinction (absorption plus scattering) spectra for many metal nanomaterials.[8] A full description of the Mie solution is beyond the scope of this tutorial and has been presented by Bohren and Huffman.[12] Willets *et al.*[2] have also provided a description as previously outlined with eqn (1)–(4). However, the frequency domain calculation of the Mie extinction, $E(\lambda)$, is given by eqn (2), where λ is the wavelength of incident radiation onto a sphere with radius, a.[2] The finite polarizable elements that can interact with the field are noted as N. The imaginary component of the wavelength-dependent dielectric is ε_i and the real component is ε_r. There is also a shape factor, χ, which describes the ease at which electrons can be polarized for a particular geometry. The shape factor is 2 for a sphere and greater than 2 for a spheroid with the exact value being dependent on the aspect ratio. Nonspherical or nonspheroid geometries require numerical methods such as discrete dipole approximation (DDA) or finite-difference time-domain (FDTD) to simulate extinction spectra,[6,13] and different shape factors are included in such calculations.

Extinction of a sphere with radius a.

$$E(\lambda) = \frac{24\pi^2 N a^3 {\varepsilon_{out}}^{3/2}}{\lambda \ln(10)}\left[\frac{\varepsilon_i(\lambda)}{(\varepsilon_r(\lambda)+\chi\varepsilon_{out})^2+\varepsilon_i(\lambda)^2}\right] \quad (2)$$

This compositional dependence on the LSPR frequency has been experimentally demonstrated in many systems. For example, Au nanospheres[6] with a diameter of 48 nm have a LSPR peak position of 533 nm in water, whereas Ag nanospheres[14] of comparable size have a LSPR peak position that is nearly 100 nm blue-shifted relative to the Au nanospheres. This blue shift is consistent with the different dielectric functions of Au and Ag. Zoric *et al.*[15] also confirmed a LSPR dependence on composition by studying nanodisks of constant size but varying composition, with Au, Pt, and Al nanodisks exhibiting different peak LSPR frequencies. For example, an Au disk with a 68 nm diameter exhibits an LSPR maximum 1.0 eV or more lower than a Pt or Al disk of the same diameter. Finally, McMahon *et al.* studied the "poor" plasmonic metals Al, Ga, In, Sn, Tl, Pb, and Bi and found that the spectral response of each metal was unique when particle size and shape were held constant.[11] All of these metals except Bi were found to provide enhancements of the electromagnetic field in the UV on the order of 10^3 or greater, which is comparable to that of Au and Ag in the visible range. However, the synthesis of these non-traditional metals in nanoparticulate form is a challenge. These metals are often more difficult to synthesize from their salt precursors, typically requiring the use of harsh reducing agents such as *n*-butyllithium. This necessity leads to difficulties in controlling the reduction kinetics and subsequent product morphology. Additionally, the tendency of these metals to oxidize diminishes their long-term stability. With size and structural control required for nanomaterials in colloidal plasmonics, there are many practical hurdles to overcome before these non-traditional metals see widespread application in plasmonic systems.

In addition to being dependent on the dielectric function of the metal colloid, the LSPR also depends on the dielectric constant of the surrounding medium.[2,6,13,16] Eqn (3) describes the relationship between the refractive index (RI) of the medium to the maximum scattering wavelength, where the RI of the medium, n, is related to its dielectric constant ε by $\varepsilon = n^2$.[2] Thus, any change in the surrounding environment that results in a change in the local RI experienced by the nanoparticle will result in a shift in the LSPR wavelength, $\Delta\lambda_{max}$. The bulk RI response is m, the distance from the particle is d, and the electromagnetic field decay length is given by l_d.

Relationship between RI and LSPR position.

$$\Delta\lambda_{max} = m\Delta n\left[1 - \exp\left(\frac{-2d}{l_d}\right)\right] \quad (3)$$

Experimentally, RI sensitivity is found by measuring the LSPR maximum wavelength of the sample in different dielectric

media and then finding the slope from the plot of RI *versus* LSPR maximum wavelength. Additionally, figure of merit, FOM = RI sensitivity/full width at half maximum (fwhm), is often calculated to standardize RI sensitivities. For more information on these calculations, see the work by Mayer *et al.*[5] On account of the sustained LSPR possible on metallic nanoparticles and their sensitivity to changes in RI, many applications in chemical sensing can be envisioned.[17] Of particular interest is the label-free optical detection of single chemical events or molecules. To achieve these goals, sensors can be designed that take advantage of the dependency of the LSPR position on both composition and changes in RI.[2,18] These types of nanoparticle sensors can be achieved from either nanoparticle dispersions or surface-immobilized nanoparticles.[18] An example of such a sensor made from metallic nanoparticles has been achieved by Liu *et al.* in which the adsorption of hydrogen on to Pd-based nanomaterials changes the RI of the local environment, resulting in a shift of the LSPR.[19] Applications of nanoparticles for LSPR sensing has been previously reviewed in detail by Mayer *et al.*[5]

Nanoparticles are also providing platforms for plasmon-enhanced spectroscopies.[2,18] For example, nanoparticle arrays on surfaces can serve as platforms to enhance both the excitation and Raman signal of chemical entities due to the electromagnetic field enhancements that result from plasmonic resonances.[20] The Raman scattering cross section can be enhanced by metallic nanoparticles; however, the particles must have a structure and composition that enables the LSPR to exist at wavelengths of interest for spectroscopic applications.[18] Eqn (4) describes the enhancement factor for surface-enhanced Raman spectroscopy (SERS) as a function of the wavelength of laser radiation, $EF_{SERS}(\omega_v)^2$ Both the incident excitation, $E_{out}(\omega)$, and the Stokes shifted Raman, $E_{out}(\omega - \omega_v)$, electromagnetic fields are enhanced relative to the localized electromagnetic field of the nanoparticle, E_0, yielding a total enhancement of approximately E^4 for most Raman bands.

Enhancement factors for SERS.

$$EF_{SERS}(\omega_v) = \frac{\left|E_{out}(\omega)^2\right|\left|E_{out}(\omega - \omega_v)^2\right|}{E_0{}^4} \approx E^4 \qquad (4)$$

Like LSPR position, LSPR line width is dependent on particle size, shape, and local environment. LSPR line width is measured as the fwhm of the resonance, and electron-surface scattering and radiation damping can cause broadening of this fwhm. Typically, electron-surface scattering will dominate at smaller particle sizes and radiation damping will dominate at larger particle sizes. For spherical particles less than 20 nm in size, the scattering of electrons at the surface is negligible; therefore, minimal broadening is observed. However, significant broadening is observed as particles either increase in anisotropy or increase in size. For example, a nanorod with a dimension less than 20 nm can still have a volume such that efficient scattering will occur. For particles greater than 100 nm in size, where radiation damping effects are large, it has been demonstrated that the LSPR linewidth is dependent on the RI of the medium, including solvents and ligands.[21]

In both SERS and RI sensing applications, there exist a best plasmon resonance which is wavelength dependent (eqn (2)).[22] For example, the magnitude of enhancement for SERS depends on the frequency match of both the LSPR maximum to the incident laser irradiation and the LSPR maximum to the Raman signal. The ability to control the position of the LSPR through the size and composition of nanoparticles provides many options and opportunities to design effective platforms for sensing applications. On account of their LSPR maxima in the visible region, Au and Ag nanoparticles are some of the most widely studied platforms, with the scattering cross section of Ag being greater than Au and in fact having the strongest plasmonic coupling with light compared to all metals. Regardless of the composition, achieving a desired LSPR wavelength through size control alone may not always be possible. For example, Au nanoparticles with a diameter of 9 nm have an LSPR maximum in water of 516 nm. Increasing their size to 15 nm, results in a 3 nm red shift of the LSPR maximum. A further increase in size to 22 nm results in only a 1 nm red shift to 521 nm.[6] Many applications require excitation with near-infrared light. Although further increases in particle size lead to a further red shift of the LSPR, both the contribution of scattering to the overall extinction and the LSPR linewidth increase,[6] which may be undesirable depending on the application.

Alloyed nanoparticles provide new opportunities in colloidal plasmonics on account of their composition-dependent optical and chemical properties. For example, the range over which the LSPR maximum can be tuned can be greater through compositional control than what can be attained through size control of monometallic nanoparticles, and they offer diversity in function. A classical example of plasmonic tunability through control of composition is the synthesis of Au–Ag alloyed nanoparticles.[6,23] Link *et al.* found that the LSPR peak position depended linearly on the mole fraction of Au in the Au–Ag alloyed nanoparticles (Fig. 4). The LSPR blue-shifted from

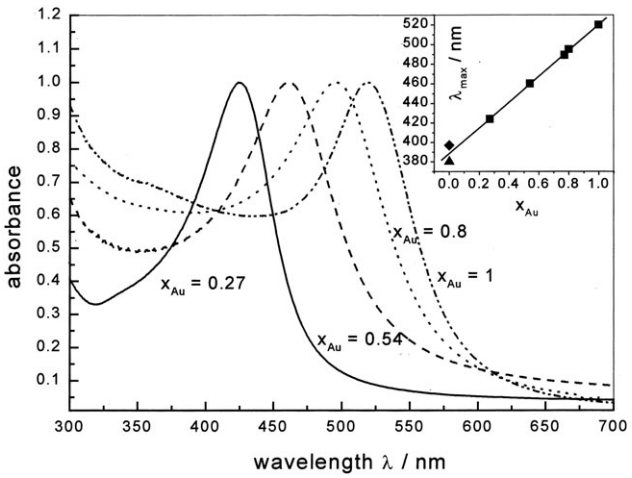

Fig. 4 UV-visible absorbance spectra of Au–Ag alloy nanoparticles as a function of Au mole fraction. Inset is a plot of LSPR position as a function of Au mole fraction, illustrating the linear relationship between position and composition in the Au–Ag alloy system. Reproduced with permission from ref. 23. Copyright 1999 American Chemical Society.

520 nm to 425 nm as the Au mole fraction for spherical particles of constant size decreased from 1 to 0.27. This approach has been extended within Ag alloy systems to include a variety of compositions and morphologies beyond spherical particles.[24]

Another material that has gained attention for its LSPR tunability is the Au–Cu alloyed nanoparticle system. In a recent example,[25] Au–Cu alloyed nanoparticles were synthesized with compositions ranging from 15% Cu to 50% Cu while maintaining a relatively constant particle size and spherical morphology. Unlike the previous Au–Ag example, the location of the LSPR maximum does not linearly correspond to the composition of the nanoparticles, but rather the increased copper content red shifts the LSPR more than expected. This result likely stems from inaccuracies in assuming a simple linear mixing for the interband contributions of Cu and Au, indicating that these alloyed systems are far more complex than can be currently modeled. However, the synthesis of bimetallic nanoparticles may reduce the cost of some plasmonic platforms. They also provide opportunities for metals which have traditionally been viewed as poor plasmonic materials to be integrated in order to achieve new chemical function, as discussed in greater detail later in this Tutorial Review.

The formation of alloyed nanoparticles is also advantageous for the opportunity to generate non-equilibrium phases due to the low temperatures and short diffusion distances that are often a staple of solution-based synthetic methods toward nanomaterials. This ability has facilitated the incorporation of other metals into plasmonic systems that would otherwise be difficult to obtain.[26] As these examples illustrate, the library of plasmonic nanoparticles is continually expanding by considering new compositions, enabling precise control of the LSPR features of the material through manipulation of nanoparticle size and composition.

From quasi-spherical nanoparticles to nanocubes, nanorods, and more: the importance of nanocrystal shape

Still, the ability to manipulate the optical properties of quasi-spherical metal colloids through particle size and composition is limited, particularly when trying to extend the LSPR maximum into the near-infrared for applications in nanomedicine and solar energy utilization. This limitation is being addressed by considering nanocrystal shape as an important parameter in the design of plasmonic colloids, as non-spherical nanoparticles can exhibit multiple LSPRs on account of lowering shape symmetry. Au nanorods, for example, exhibit longitudinal and transverse LSPRs corresponding to the long and short axes of their structure, respectively. Lowering of shape symmetry can also provide locations where electric field intensity can concentrate, colloquially known as ''hot-spots.'' These hot-spots facilitate detection of molecules, most popularly *via* SERS, at remarkably low concentrations.[2] For non-spherical nanoparticles, changes in the polarization of the irradiating light can turn on and off specific hot-spots. Polarization-dependent alterations to the extinction spectrum can be calculated through the use of an appropriate shape factor χ in eqn (2). The previous discussions of spherical and nanorod geometries were limited to dipolar surface plasmon modes; however, multiple modes do exist (*e.g.*, quadrupolar modes that arise from two dipoles in opposite direction) and are explicitly stated when relevant for our discussion of nonspherical geometries.[20]

Much of what is known about the optical properties of shape-controlled metal nanostructures has been enabled by advances in synthesis, which now provide a range of shape-controlled nanostructures as high-quality samples.[9] Shapes range from Platonic solids such as cubes and octahedra to Archimedian solids such as cuboctahedra to Catalan solids such as tetrahexahedra and rhombic dodecahedra.[27] Surfaces can be modified to have high-energy high-index facets, high angle vertices, and concavities.[28] These structures can also be tailored in their size and composition. Three synthetic parameters have been emphasized when approaching the synthesis of shape-controlled nanocrystals: the seed shape, the capping agents present, and the growth kinetics.

Many of the final structural characteristics of a nanoparticle are determined in the earliest stages of a nanomaterial synthesis. For example, *in situ* TEM studies of metal nanoparticle formation reveal that both monomer overgrowth and oriented attachment can occur simultaneously, the latter which has been rationalized for the appearance of crystal defects in nanoparticles.[29] Such crystal defects (*e.g.*, twin planes and stacking faults) direct what nanocrystal shapes are then synthetically accessible.[9,30] For example, single-crystalline nanocubes and octahedra form from single-crystalline seeds, whereas multiply-twinned nanorods form from pentagonally-twinned seeds. In general, the use of a seed with a specific symmetry can facilitate the synthesis of a larger particle with the same or similar symmetry. The role of seed shape on final nanocrystal structure has been reviewed in the works of Xia and co-workers and the general principle is summarized in Fig. 5.[9,31] Significantly, the recognition that initial seed structures direct the shapes of the final nanostructures has led to the separation of the primary nucleation step from the subsequent overgrowth phase to improve the quality and structural complexity of shape-controlled nanocrystals. Such ''seeded'' methods are now premier means to shape-controlled nanocrystals given the continued challenges in predicting and controlling the earliest stages of nanomaterial syntheses.[40]

Capping agents (*e.g.*, ligands, polymers, anions) also contribute to the final outcome from a nanomaterial synthesis. Aside from providing colloidal stability, capping agents can facilitate the preferential growth of specific facets and the adoption of a final nanocrystal shape. Several factors have been postulated to explain the dynamic role capping agents have in controlling shape, ranging from preferential adsorption onto specific facets to kinetic control of adatom addition and diffusion.[32] As ''facet blockers,'' capping agents are thought to preferentially adsorb on to specific facets of seeds. This adsorption process provides a means of thermodynamic stabilization,

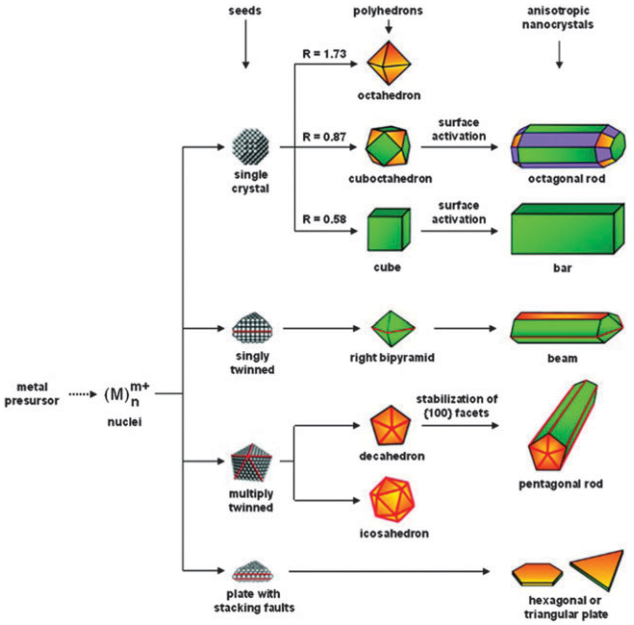

Q5 Fig. 5 Schematic illustrating the importance of the initial seed structures in the role of the final particle shape. Reproduced with permission from ref. 31. Copyright 2009 American Chemical Society.

inhibiting deposition at those sites and facilitating their expression in the final shape of the nanocrystals.[33,34] One illustration of the structure-directing effect of capping agents is from the synthesis of {111}-terminated Ag octahedra and {100}-terminated Ag nanocubes from quasi-spherical Ag seeds in the presence of citrate or poly(vinylpyrrolidone) (PVP), respectively.[33] In this example, all other synthetic parameters were held constant. The emergence of octahedra in the presence of citrate was consistent with density functional theory (DFT) calculations which found that citrate has a binding constant that is six orders of magnitude greater in adsorption to Ag(111) compared to Ag(100) on account of the favorable match of symmetry between the functional groups of citrate and the Ag(111) surface. In contrast, PVP preferentially adsorbs to {100} surfaces and {100}-terminated Ag nanocubes form.[32]

In general, capping agents have been identified that can facilitate the preferential expression of low index facets in the colloidal synthesis of noble metals, but there is still a need to identify new capping agents which can stabilize higher index surfaces in order to facilitate the synthesis of completely new nanocrystal shapes. One promising development involves the use of phage display techniques to identify tailored peptides for use as capping agents.[34] In this approach, a library of peptide sequences are screened for their binding affinity at model surfaces and those with the greatest binding affinities can then be applied as capping agents to nanoparticle syntheses. For example, the T7 (TLTTLTN) peptide preferentially binds to Pt {100} surfaces, and {100}-terminated Pt nanocubes were formed when the peptide was used as a capping agent in the synthesis of Pt nanostructures. Importantly, the structural control of peptide sequences goes beyond stabilizing low-index metal surfaces. Nanostructures with complex morphologies, such as

$$M^{a+}(\text{solution}) + e^- \xrightarrow{r} M(\text{solution}, \mu_1) \quad \text{Step 1}$$
$$M(\text{solution}, \mu_1) \xrightarrow{\Delta\mu} M(\text{crystal}, \mu_c) \quad \text{Step 2}$$

Scheme 1

Pt multipods or Ag nanowires with a spiral structure, have been achieved with peptides that preferentially bind to higher-energy surfaces or induce multiple nucleation events, respectively. These findings hint toward the possibility of greater structural control through designer capping agents.

In conjunction with these "facet blocking" effects, capping agents as well as other additives to a synthesis can manipulate the kinetics of nanoparticle growth, which in turn can alter their shape towards higher energy surfaces and morphologies not predicted by capping agent selection. Shown in Scheme 1 are two steps typically found in the growth of metal nanocrystals, where μ_1 is the chemical potential of metal atoms reduced in solution, μ_c is the chemical potential of metal atoms of the solid phase, and their difference $\Delta\mu$ is the thermodynamic driving force for crystallization (*i.e.*, the solution supersaturation).[32] In Step 1, metal precursor M^{a+} is reduced and in Step 2 metal M attaches to the crystal.

In accordance with the Thomson–Gibbs equation, excess energy from a crystallization process converts to the surface energy of crystallites at constant pressure and temperature, and recent work by Lin *et al.*[32] illustrated that in seeded growth of Au nanocrystals, an increase in supersaturation results likewise in nanocrystals with higher energy facets expressed. This control was achieved chemically in accordance with Scheme 1 by varying either the concentration of Au precursor or the reaction pH. In the case of precursor concentration, the nanocrystals adopted {111}-terminated octahedral, {111}/{100} cuboctahedral, and {100} cubic profiles with increasing supersaturation achieved by the increase in precursor. This trend is consistent with the relative surface energies, γ, of low index facets for Au (*i.e.*, $\gamma_{[111]} < \gamma_{[100]} < \gamma_{[110]}$). In the case of reaction pH, ascorbic acid was used as a reducing agent for $HAuCl_4$ in aqueous solutions containing CTAB and the reduction rate is increased at high pH. Thus, the Au nanocrystals adopt a cubic shape at low pH and trisoctahedral and rhombic dodecahedral shapes, with {331} and {110} facets respectively, at higher pH. By surveying recent manuscripts on shape-controlled nanocrystal synthesis, Lin *et al.* concluded that manipulation of synthetic parameters that adjust solution supersaturation represents a general means of morphology control.[32] However, we note that this control is likely to be most easily applied to seeded methods as the primary nucleation step results in a dramatic reduction in supersaturation. We also note that the interplay of different components in a synthesis can alter reduction processes, and thus supersaturation, in seemingly unpredictable ways and deconvoluting these interactions is at the forefront of research in the area of nanomaterial synthesis.

In fact, Mirkin and co-workers recently outlined the rules governing Au nanocrystal formation in an aqueous, seed-mediated approach by decoupling the intertwined roles of seed

morphology, capping agent, and growth kinetics.[35] These principles can be applied to the shape-controlled synthesis of metal nanocrystals with other compositions, which in turn will reveal new optical properties. For example, Pd nanocrystals typically have LSPRs in the UV region. However, under kinetically controlled growth conditions, Pd nanoplates can be prepared that have LSPRs that extend as far as 500 nm.[9] On account of their LSPRs extending into the visible region, these structures may be useful for LSPR-sensing and the storage of hydrogen simultaneously. As these synthetic strategies are applied to new compositions, it is envisioned that novel nanoparticles will be designed for new applications in colloidal plasmonics.

Moreover, these high-quality samples of shape-controlled nanocrystals are appropriate platforms for studying the fundamental optical properties of metal colloids in depth. Historically, ensemble measurements were collected to elucidate the influence of size, shape, and dielectric environment on the optical properties of colloidal metallic nanoparticles. However, this approach fails to provide a complete description of effects on account of the unavoidable, albeit generally small degree of, heterogeneity in samples of size- and shape-controlled metal nanoparticles.[16,21,22] Small changes in both size and shape can lead to significant changes in the maximum LSPR frequency and line width. As the ability to design nanocrystals for particular sensing applications requires knowledge of these effects, single particle studies are necessary in order to determine the effects of all factors.[16,22]

Correlation of optical properties and structural features at a single particle level has been accomplished by several groups.[13,21,22,36,37] Methods to correlate optical properties and structure include those developed by Wang *et al.*[38] in which dark field scattering and subsequent TEM images of Ag nanoparticles were collected. Guiton *et al.* have also correlated optical measurements and plasmon mapping of Ag nanorods to yield spatial maps of the LSPR on the nanorods.[39] Such single particle studies have enabled the quantification of size, shape, and dielectric effects on optical properties of metallic nanocrystals.[22] For example, collecting scattering spectra from individual silver nanobars with varying lengths, the LSPR was found to red shift by 300 nm when their length increased from 100 nm to 200 nm.[40] These studies have yielded three primary design considerations beyond size, composition and local dielectric environment and can generally be considered as shape effects.

The first shape effect to consider in the design process is the correlation between particle symmetry and the number of resonances which will be observed. For example, the spectrum of quasi-spherical Au nanoparticles will include two resonances: a main dipole resonance and a weaker quadrupole resonance as a shoulder. Lowering the symmetry of the nanoparticles will introduce additional resonances on account of the different ways in which light can be polarized by a structure.[41] For example, Au nanorods display both longitudinal and transverse dipolar modes with multipolar modes possible with higher aspect ratios consistent with the long and short axes of the rods.[6] This observation is a consequence of the difference in restoring force for electron oscillation along each axis.[4] Likewise, other nanocrystal geometries will yield multiple symmetries for dipole resonance consistent with their shape, giving rise to more peaks.

The second shape effect to consider in the design process is that of plasmon length. Plasmon length is the distance over which the collective oscillations occur and is enabled by both the size and shape of a particle. As demonstrated by Ringe *et al.*, the plasmon length of a structure determines both the position and line width of the dipolar LSPR and is an intrinsic, and possibly universal, parameter to define plasmonic nanostructures.[17] Specifically, the individual light scattering spectra of 500 different-sized Au nanocubes, decahedra, icosohedra, octahedra, and truncated bitetrahedra were measured and normalized against both their side lengths and plasmon lengths (determined from numerical calculations and plasmon field mapping). No correlation was found with side length (Fig. 6a). However, nanostructures of different shape but similar plasmon lengths have similar LSPR spectra (Fig. 6b). Prior to this work, size parameters were arbitrarily established when comparing various shaped nanocrystals to their LSPR, making comparisons between different structural classes difficult (*e.g.*, the LSPRs of Au nanorods were analyzed in terms of aspect ratio, whereas the LSPRs of nanocubes were analyzed in terms of edge length). Plasmon length and the use of plasmon length aspect ratios allows for a true comparison between different shaped Au (and likely other) nanocrystals in order to determine the size and shape necessary to yield a particular optical response.

The third shape effect to consider in the design process is that of subtle differences, *e.g.*, the blunting of corners. As outlined by Ringe *et al.*, the concept of plasmon length can only be applied to structures with well-formed vertices, as slight heterogeneities at these sites can induce large changes in both

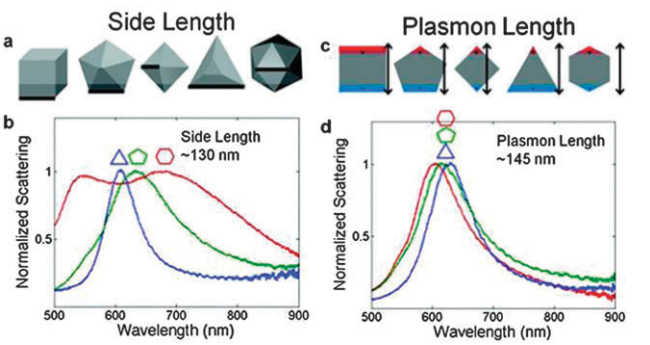

Fig. 6 Comparison between the side length and plasmon length as descriptors of nanoparticle size. (a) Definition of the side length for the shapes analyzed. Solid bars are used to indicate side length. (b) Representative single-particle light scattering spectra for Au triangles (blue), decahedra (green), and icosahedra (red) with side lengths of 130 nm. (c) Definition of plasmon length for the shapes analyzed. Arrows are used to indicate plasmon direction. (d) Representative single-particle light scattering spectra for Au triangles (blue), decahedra (green), and icosahedra (red) of similar or plasmon length. Reproduced with permission from ref. 17. Copyright 2012 American Chemical Society.

the maximum LSPR position and line width.[42] For example, single particle studies found that Ag nanobars exhibit a maximum LSPR frequency that is red shifted 80 nm on average compared to similarly sized Au nanorice, which have blunted tips.[40] This red shift is attributed to the greater accumulation of charge at sharp features, which reduces the restoring force for electron oscillation. Subtle structural differences such as rounding of corners also often account for the broader resonances from ensemble measurements compared to single particle spectra.[43] Moreover, such subtle structural differences can determine whether or not a given structure will be useful in an application as the largest induced polarization and largest electric field enhancement will occur at the sharp tips of nanocrystals. For example, Nehl *et al.* demonstrated from single particle spectroscopy measurements that Au nanostars have multiple resonances which correspond to the different tips of the branched structures.[37] Calculated electric field enhancements indicate localization at the sharp features, with an orientation dependence on LSPR wavelength and field enhancement demonstrated. On account of their sharp tips, Au nanostars have been studied as platforms for a variety of sensing and biomedical applications. However, the subtle variations in both tip sharpness and structural symmetry from one particle to the next makes it challenging to use these (and many other) nanostructures in applications which require a high degree of structural homogeneity from one synthetic batch to the next.

Finally, just as quasi-spherical metal nanoparticles of different compositions display sensitivity to changes in their local environment,[42,44] so do shape-controlled plasmonic colloids. Moreover, during the course of single-particle analyses various substrate effects on the LSPR of shape-controlled metal nanocrystals have been revealed. For example, Ringe *et al.* observed a LSPR shift for Au and Ag nanocubes on formvar *versus* silicon nitride substrates. For equivalently shaped Au and Ag nanocubes with similar corner sharpness, Ringe *et al.* reported an LSPR increase from 475 nm on formvar to 524 nm on silicon nitride for Ag and an LSPR increase from 583 nm on formvar to 603 nm on silicon nitride for Au.[16] They also presented FDTD calculations for an Au nanocube on a glass substrate that indicated an effect of particle-substrate distance on the optical response of the nanocubes. For example, the LSPR of the four corners of an Au nanocube that are in close proximity to a glass substrate will red-shift from 542 nm to 552 nm when the distance from the substrate decreases from infinity in air to 2 nm from the substrate. Decreasing the particle-substrate distance to 0 nm resulted in a further LSPR red-shift to 562 nm.[22] Adjacent particles also affect the local environment. Therefore, interparticle distances must be considered also, and the interactions between particles can be used to create unique hot-spots for sensing applications.[44]

These examples illustrate that the ability to manipulate the optical properties of metal nanostructures for applications in colloidal plasmonics is enhanced through the consideration of shape-controlled nanostructures. As the ability to achieve high quality samples *via* solution-based methods has been demonstrated, our understanding of the fundamental optical properties of metal colloids has improved. For example, the plasmon length enabled by a given nanocrystal shape has emerged as a universal descriptor of structure. Also, the subtle differences between nanostructures are being given greater attention as these structural differences can have a dramatic impact on the optical properties and overall usefulness of a structure in a given application.

Bringing shape and composition together: new colloidal plasmonic platforms

As discussed, control of nanoparticle size and composition provides a means to manipulate the LSPR properties of a nanostructure. Control of nanocrystal shape enhances this ability, in which the number, width, and location of extinction peaks can be tailored to achieve designer plasmonic colloids. Now, new multi-metallic platforms are being envisioned which bring shape and composition together in the form of architecturally controlled nanostructures in order to achieve new function. The concept of architecturally controlled structures to enhance the optical properties of plasmonic colloids, however, is not new and is represented well with the example of core@shell SiO_2@Au nanoshells. Prepared by Halas *et al.* by deposition of Au onto SiO_2 colloids, it was found that adjusting the thickness of the Au shell alters the hybridization of the inner cavity and outer sphere plasmons.[45] As shell thickness decreases, coupling between the interior and exterior plasmons strengthens, leading to a red shift in the LSPR.[46] By changing the composition of the core to Fe_xO_y, a magnetic response can be built into such nanoshells.[47] Also, control of the shell composition can bring about new function. For example, quasi-spherical Pd nanoparticles have LSPRs too far into the UV region of the electromagnetic spectrum to be used as a platform for sensing *via* SERS; however, Pd can be incorporated into Au in the form of SiO_2@Au/Pd nanoshells, which provides a maximum LSPR near 750 nm.[48] As a result, these nanoshells are a suitable platform for SERS, where the Pd component serves as a catalyst for the hydrodechlorination of 1,1-dichloroethene in water which was monitored spectroscopically under operating conditions.

The ability to tune the optical properties and function of nanomaterials through this core@shell architecture has motivated many to achieve related structures in bimetallic form, where metal nanocrystals rather than SiO_2 colloids serve as seeds in a synthesis. Through the use of shape-controlled nanocrystals as seeds to which a second metal will be deposited, architecturally controlled nanocrystals are being achieved that utilize *both* composition and shape control to achieved tailored plasmonic colloids.[26] For example, the optical properties of core@shell bimetallic nanocrystals can be manipulated by shell thickness as the dielectric constants of both metals contribute to the overall response. For example, the LSPR of Au@Pd nanobars blue-shift with increasing thickness of the Pd

shells and can display higher sensitivities to changes in RI than Au nanobars of similar size.[49] By coupling a metal traditionally viewed as poor for plasmonic applications, Pd, to a good plasmonic metal, Au, both enhanced properties and new function are emerging.

Innovative synthetic techniques are also being developed to move bimetallic nanocrystals beyond conformal core@shell architectures.[26] Bimetallic nanocrystals with spatially localized regions of metal or hollow features have been achieved and display favorable optical properties for many applications.[50,51] For example, Au–Ag nanocages are synthesized through galvanic replacement between Au precursors and shape-controlled Ag seeds. The position of their LSPR depends on the extent of exchange as well as the size of the initial Ag template, and these Au–Ag nanocages are finding use in many photothermal and nanomedicine applications on account of their strong absorption far into the near-IR.[52]

Simultaneous reduction of two metal precursors in the presence of shape-controlled seeds also provides access to new bimetallic nanostructures with applications in colloidal plasmonics.[26] For example, this "seed-mediated co-reduction" approach enables the synthesis of symmetrically branched bimetallic nanocrystals that can have high sensitivity to changes in RI.[26] Shown in Fig. 7 is an example of eight-branched Au/Pd nanostructures with

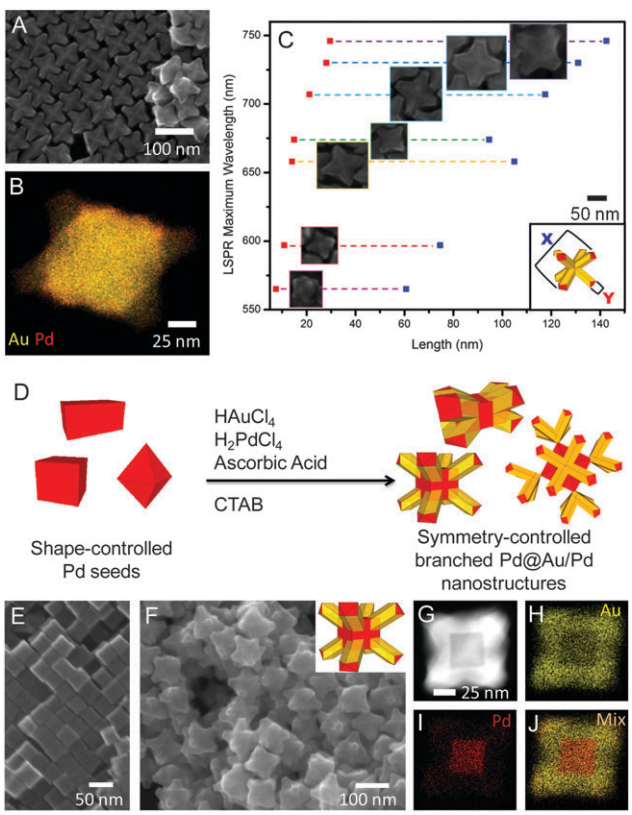

Fig. 7 (A) SEM image and (B) STEM-EDX mapping of octopods. (C) Plot illustrating the LSPR maximum wavelength as a function of morphology. (D) Schematic illustrating the synthesis of branched nanostructures. (E) SEM image of cubic Pd seeds and (F) resulting octopods. (G–J) STEM and elemental mapping of octopods. Reproduced with permission from ref. 26. Copyright 2013 American Chemical Society.

O_h symmetry, termed "octopods", prepared by co-reducing Au and Pd precursors in the presence of Au seeds. Control of branch length for the Au/Pd octopods is possible by adjusting the total concentration of metal precursors relative to the number of seeds during co-reduction.[26] As the length of the branches increases, a red shift is observed (Fig. 7C). Interestingly, co-reducing the Au and Pd precursors in the presence of various Pd seeds allowed the symmetry relationships between seeds and branched nanocrystals to be established (Fig. 7D–J).[26] These studies show that it is possible to tailor the symmetry of branched nanostructures, which could be useful in the design of new plasmonic platforms as light can concentrate at features with a small radius of curvature. Finally, seed-mediated co-reduction has facilitated the synthesis of other shape-controlled bimetallic structures, including Cu_3Au, Cu_3Pt, and Cu_3Pd nanorods with tunable optical properties.[53] For more information on how shape and composition can be integrated into individual nanocrystals to achieve new plasmonic colloids, see our recent perspective which highlights advances in the seed-mediated synthesis of bimetallic nanostructures.[26]

Concluding thoughts

The recent advances in the area of plasmonic colloids result from the ability of scientists both to exploit a diversity of reaction conditions to obtain architecturally controlled nanostructures and to develop the analytical and modeling techniques necessary to understand their optical properties. From these studies, a number of guiding principles have emerged to direct the rational design of plasmonic colloids. First, composition sets the short wavelength boundary for the LSPR, the strength of plasmonic coupling with light, and the chemical function (*e.g.*, magnetic, catalytic, *etc.*) of a plasmonic colloid. The first two of these features biased early research in colloidal plasmonics to primarily Au and Ag nanostructures. However, advances in the synthesis of nanostructures with shape- and architectural control and the desire for plasmonic colloids with added function have moved researchers to consider new compositions. Second, the position and line width of the LSPR is governed by the plasmon length enabled by the size and shape of a nanocrystal. This realization should facilitate the identification of the most appropriate structure in terms of light absorption and scattering prior to synthesis by modeling the optical properties of potential nanocrystals. Third, the shape of a metal nanocrystal will determine the number of resonances displayed. This feature of shape-controlled nanocrystals can provide greater versatility when integrating a nanostructure into an application (*e.g.*, two different wavelengths of light can be employed). This feature can also provide new function through selective activation of resonances to trigger a particular chemical or physical event. Fourth, subtle differences from one structure to the next can bring about large differences in the optical properties displayed and must be considered and mitigated when applying nanostructures in various applications. Fifth, the local environment of a nanostructure influences the position and symmetry of the LSPR. This feature can lead to misinterpretations of observations as something as simple as a ligand exchange process can result in an LSPR shift.

However, this high sensitivity also makes plasmonic colloids a potentially powerful platform for detection of single chemical events or molecules.

Current efforts are directed toward gaining better understanding of how composition and architecture come together to yield colloids with tunable optical properties. Although existing synthetic methodologies have achieved greater product uniformity in terms of size, shape, and composition, current protocols often do not have the synthetic robustness desirable for industrial implementation. Thus, it will be necessary to develop synthetic protocols that result in products with a high degree of reproducibility in terms of composition, yield, and purity that is independent of the location of the laboratory where the synthesis occurs or chemical lots of reagents.[54] These improvements are necessary in a field where small changes in nanostructure or distances between particles can lead to very large changes in optical signatures. Moreover, as the complexity of plasmonic colloids increases, nanostructure characterization poses a challenge. It will increasingly become necessary to employ advanced electron microscopy techniques to achieve three-dimensional images of structures in conjunction with compositional analysis. Then, with improved methods for modeling the optical properties of such structures, it should be possible to provide a complete view of the interplay between composition, crystal structure, and morphology within advanced plasmonic colloids.

Although plasmonic colloids with complex compositions and architectures are becoming more commonplace, there currently exists an application-nanostructure mismatch. That is, applications are often built around the plasmonic properties of existing nanomaterials rather than designing the best platform for a specific application. It has been previously outlined[10] that the next step is to invert this relationship and model what structural and compositional parameters within a nanomaterial are necessary for a specific application then target its synthesis. For this goal to be realized, partnerships between those advancing the synthesis, characterization, and modeling of nanomaterials must be forged to address the complexity of new plasmonic platforms. As these challenges are addressed, the rational design and synthesis of new plasmonic colloids for applications ranging from nanoelectronics and catalysis to energy storage and biomedical imaging will be possible.

Acknowledgements

Support comes from Indiana University (IU) – Bloomington start-up funds, IU's Office of the Vice President for Research and the Office of the Vice Provost for Research through the Faculty Research Support Program, the Alfred P. Sloan Foundation, the Cottrell Scholar Program (Research Corporation), and NSF Award CHE-1306853.

Notes and references

1 http://www.katenicholsstudio.com/looking-glass.php.
2 K. A. Willets and R. P. Van Duyne, *Annu. Rev. Phys. Chem.*, 2007, **58**, 267–297.
3 E. C. Dreaden, A. M. Alkilany, X. Huang, C. J. Murphy and M. A. El-Sayed, *Chem. Soc. Rev.*, 2012, **41**, 2740–2779.
4 S. A. Maier and H. A. Atwater, *J. Appl. Phys.*, 2005, **98**, 011101.
5 K. M. Mayer and J. H. Hafner, *Chem. Rev.*, 2011, **11**, 3828–3857.
6 S. Link and M. A. El-Sayed, *J. Phys. Chem. B*, 1999, **103**, 8410–8462.
7 J. Gong, G. Li and Z. Tang, *Nano Today*, 2012, **7**, 564–585.
8 E. Ringe, J. Zhang, M. R. Langille, C. A. Mirkin, L. D. Marks and R. P. Van Duyne, *Nanotechnology*, 2012, **23**, 444005.
9 Y. Xia, Y. Xiong, B. Lim and S. E. Skrabalak, *Angew. Chem., Int. Ed.*, 2009, **48**, 60–103.
10 T. W. Odom and C. L. Nehl, *ACS Nano*, 2008, **2**, 612–616.
11 J. M. McMahon, G. C. Schatz and S. Gray, *Phys. Chem. Chem. Phys.*, 2013, **15**, 5415–5423.
12 C. F. Bohren and D. R. Huffman, *Absoption and scattering of light by small particles*, Wiley, New York, 2008.
13 A.-I. Henry, J. M. Bingham, E. Ringe, L. D. Marks, G. C. Schatz and R. P. Van Duyne, *J. Phys. Chem. C*, 2011, **115**, 9291–9305.
14 C. M. Cobley, M. Rycenga, F. Zhou, F.-Z. Li and Y. Xia, *J. Phys. Chem. C*, 2009, **113**, 16975–16982.
15 I. Zoric, M. Zach, B. Kasemo and C. Langhammer, *ACS Nano*, 2011, **5**, 2535–2546.
16 E. Ringe, J. M. McMahon, K. Sohn, C. Cobley, Y. Xia, J. Huang, G. C. Schatz, L. D. Marks and R. P. Van Duyne, *J. Phys. Chem. C*, 2010, **114**, 12511–12516.
17 E. Ringe, M. R. Langille, K. Sohn, J. Zhang, J. Huang, C. A. Mirkin, R. P. Van Duyne and L. D. Marks, *J. Phys. Chem. Lett.*, 2012, **3**, 1479–1483.
18 M. E. Stewart, C. R. Anderton, L. B. Thompson, J. Maria, S. K. Gray, J. A. Rogers and R. G. Nuzzo, *Chem. Rev.*, 2008, **108**, 494–521.
19 N. Liu, M. L. Tang, M. Hentschel, H. Giessen and A. P. Alivisatos, *Nat. Mater.*, 2011, **10**, 631–636.
20 X. Lu, M. Rycenga, S. E. Skrabalak, B. Wiley and Y. Xia, *Annu. Rev. Phys. Chem.*, 2009, **60**, 167–192.
21 G. V. Hartland, *Chem. Rev.*, 2011, **111**, 3858–3887.
22 E. Ringe, B. Sharma, A.-I. Henry, L. D. Marks and R. P. Van Duyne, *Phys. Chem. Chem. Phys.*, 2013, **15**, 4110–4129.
23 S. Link, Z. L. Wang and M. A. El-Sayed, *J. Phys. Chem. B*, 1999, **103**, 3529–3533.
24 M. Rycenga, C. M. Cobley, J. Zeng, W. Li, C. H. Moran, Q. Zhang, D. Qin and Y. Xia, *Chem. Rev.*, 2011, **111**, 3669–3712.
25 N. E. Motl, E. Ewusi-Annan, I. T. Sines, L. Jensen and R. E. Schaak, *J. Phys. Chem. C*, 2010, **114**, 19263–19269.
26 C. J. DeSantis, R. G. Weiner, A. Radmilovic, M. M. Bower and S. E. Skrabalak, *J. Phys. Chem. Lett.*, 2013, **4**, 3072–3082.
27 H. Zhang, M. Jin, Y. Xiong, B. Lim and Y. Xia, *Acc. Chem. Res.*, 2013, **46**, 1783–1794.
28 H. Zhang, M. Jin and Y. Xia, *Angew. Chem., Int. Ed.*, 2012, **51**, 7656–7673.
29 J. M. Yuk, J. Park, P. Ercius, K. Kim, D. J. Hellebusch, M. F. Crommie, J. Y. Lee, A. Zettl and A. P. Alivisatos, *Science*, 2012, **336**, 61–64.

30 T. C. R. Rocha and D. Zanchet, *J. Phys. Chem. C*, 2007, **111**, 6989–6993.
31 S. E. Skrabalak and Y. Xia, *ACS Nano*, 2009, **3**, 10–15.
32 H. X. Lin, Z.-C. Lei, Z.-Y. Jiang, C.-P. Hou, D.-Y. Liu, M.-M. Xu, Z.-Q. Tian and Z.-X. Xie, *J. Am. Chem. Soc.*, 2013, **135**, 9311–9314.
33 X. Xia, J. Zeng, Q. Zhang, C. H. Moran and Y. Xia, *J. Phys. Chem. C*, 2012, **116**, 21647–21656.
34 B. D. Briggs and M. R. Knecht, *J. Phys. Chem. Lett.*, 2012, **3**, 405–418.
35 M. R. Langille, M. L. Personick, J. Zhang and C. A. Mirkin, *J. Am. Chem. Soc.*, 2012, **134**, 14542–14554.
36 P. S. Kumar, I. Pastoriza-Santos, B. Rodriguez-Gonzalez, F. J. G. de Abajo and L. M. Liz-Marzán, *Nanotechnology*, 2008, **19**, 015606.
37 C. L. Nehl, H. Liao and J. H. Hafner, *Nano Lett.*, 2006, **6**, 683–688.
38 Y. Wang, S. Eswaramoorthy, L. Sherry, J. Dieringer, J. Camden, G. Schatz, R. Van Duyne and L. Marks, *Ultramicroscopy*, 2009, **109**, 1110–1113.
39 B. S. Guiton, V. Iberi, S. Li, D. N. Leonard, C. M. Parish, P. G. Kotula, M. Varela, G. C. Schatz, C. J. Pennycook and J. P. Camden, *Nano Lett.*, 2011, **11**, 3482–3488.
40 B. J. Wiley, Y. Chen, J. M. McLellan, Y. Xiong, Z.-Y. Li, D. Ginger and Y. Xia, *Nano Lett.*, 2007, **7**, 1032–1036.
41 A. L. Schmucker, N. Harris, M. J. Banholzer, M. G. Blaber, K. D. Osberg, G. C. Schatz and C. A. Mirkin, *ACS Nano*, 2010, **4**, 5453–5463.
42 K. L. Kelly, E. Coronado, L. L. Zhao and G. C. Schatz, *J. Phys. Chem. B*, 2003, **107**, 668–677.
43 B. J. Wiley, S. H. Im, Z.-Y. Li, J. McLellan, A. Siekkinen and Y. Xia, *J. Phys. Chem. B*, 2006, **110**, 15666–15675.
44 L. Slaughter, W.-S. Chang and S. Link, *J. Phys. Chem. Lett.*, 2011, **2**, 2015–2023.
45 H. Wang, D. W. Brandl, P. Nordlander and N. J. Halas, *Acc. Chem. Res.*, 2006, **40**, 53–62.
46 R. Bardhan, S. Lal, A. Joshi and N. J. Halas, *Acc. Chem. Res.*, 2011, **44**, 936–946.
47 C. S. Levin, C. Hofmann, T. A. Ali, A. T. Kelly, E. Morosan, P. Nordlander, K. H. Whitmire and N. J. Halas, *ACS Nano*, 2009, **3**, 1379–1388.
48 K. N. Heck, B. G. Janesko, G. E. Scuseria, N. J. Halas and M. S. Wong, *J. Am. Chem. Soc.*, 2008, **130**, 16592–16600.
49 K. Zhang, Y. Xiang, X. Wu, L. Feng, W. He, J. Liu, W. Zhou and S. Xie, *Langmuir*, 2008, **25**, 1162–1168.
50 W. Wang, M. Dahl and Y. Yin, *Chem. Mater.*, 2012, **25**, 1179–1189.
51 S. E. Skrabalak, J. Chen, Y. Sun, X. Lu, L. Au, C. M. Cobley and Y. Xia, *Acc. Chem. Res.*, 2008, **41**, 1587–1595.
52 Y. Xia, W. Li, C. M. Cobley, J. Chen, X. Xia, Q. Zhang, M. Yang, E. C. Cho and P. K. , *Acc. Chem. Res.*, 2011, **44**, 914–924.
53 S. Chen, S. V. Jenkins, J. Tao, Y. Zhu and J. Chen, *J. Phys. Chem. C*, 2013, **117**, 8924–8932.
54 R. E. Schaak and M. E. Williams, *ACS Nano*, 2012, **6**, 8492–8497.

